

THE BROAD-BAND IMPEDANCE BUDGET IN THE ACCUMULATOR RING OF ALS-U PROJECT*

D. Wang[†], K. Bane, D. Li, T. Luo, S. De Santis, M. Venturini
Lawrence Berkeley National Laboratory, Berkeley, USA

Abstract

Design work is underway for the upgrade of the Advanced Light Source (ALS-U) to a diffraction-limited soft x-rays radiation source. It consists of an accumulator and a storage ring. In both rings, coupling-impedance driven instabilities need careful evaluation to ensure meeting the machine high-performance goals. This paper presents the broad-band impedance budget of the accumulator ring both longitudinally and transversely. The budget includes the resistive wall impedance as well as the geometric impedance from the main vacuum components. Our calculations primarily rely on electromagnetic simulations with the CST code; when possible validation has been sought against analytical modeling, typically in the low-frequency limit, and good agreement generally found. Collective-instability current thresholds are also discussed.

INTRODUCTION

ALS-U is under design to upgrade the existing Advanced Light Source (ALS) at LBNL to a diffraction-limited soft x-rays radiation source, with brightness about tow orders of magnitude higher than that of ALS. The upgrade program includes the replacement in the storage ring (SR) of the existing triple-bend achromat with a multi-bend achromat lattice and the installation of a new low emittance accumulator ring (AR) in the existing tunnel, with the purpose of enabling swap-out injection into the SR small aperture [1].

One of the significant factors potentially limiting performance in a ring is the beam's interaction with electromagnetic fields induced in a vacuum chamber by the beam itself, which is described with short-range wakefield (time domain) or, equivalently, broad-band (BB) impedance (frequency domain) [2]. BB impedance in the ring is caused by resistive wall as well as the localized elements such as BPM, RF cavity, pump screens, etc. BB impedance can affect the machine performance/operation in several ways including overheating of vacuum chamber components and giving rise to instability of beam motion, leading to deterioration of the beam quality and limitation of the beam intensity [3].

In this paper, the BB impedance budget of the AR in the ALS-U has been extensively surveyed using a combination of analytical models and numerical simulations. The total impedance budget has been computed for the beam with nominal bunch length of 5 mm rms. We also calculated the short range wakefield of a 1mm rms drive beam to serve as the pseudo-Green function for beam dynamics study. The

collective-instability study to determine the single bunch current thresholds for both longitudinal and transverse instability is performed by *elegant* [4].

IMPEDANCE MODELING

The BB impedance comes from the resistive wall and the geometric components. We calculate the resistive wall impedance with analytical formulas [5] and determine the geometry impedance with the numerical solver CST Particle Studio [6].

Resistive Wall Impedance

The resistive wall impedance is an important part in the impedance model. The lattice design of the accumulator ring is TBA periodic structure, with three bending magnets in each sector. There are 12 sectors and the total the circumference $C \approx 182$ m. Figure 1 shows the layout of a normal arc section and Table 1 shows the characteristics of the three different types of vacuum chamber sectors for the sector shown in Fig. 1.

We adopt the common infinite-thickness wall, DC conductivity resistive-wall model. In an elliptical chamber the impedance in longitudinal and transverse plane are [4]:

$$Z_{||}(\omega) = \frac{Z_0 \delta \omega}{4\pi bc} (\text{sign}(\omega) - i) \times F_{YOKOYA} \quad (1)$$

$$Z_{\perp}(\omega) = \frac{Z_0 \delta \omega}{2\pi b^3} (\text{sign}(\omega) - i) \times F_{YOKOYA}, \quad (2)$$

with b is the smaller chamber half-axis, $\delta = \sqrt{2/\mu_0 \sigma_c |\omega|}$ the skin depth depending on the material conductivity, F_{YOKOYA} the Yokoya geometry factors [7]. For AR dipole chamber with $2a = 40\text{mm}$ major and $2b = 14\text{mm}$ minor axis, the Yokoya's factors are $F_z = 0.98$ (longitudinal), $F_{d,x} = 0.43$ (dipole, horizontal), $F_{d,y} = 0.83$ (dipole, vertical), and $F_q = 0.4$ (quadruple).

Table 1: Types and Features of the Normal Arc Section in the Accumulator Ring as Shown in Fig. 1

Type	ID (mm)	Profile	Length (m)	Material
Dipole	14(y) 40(x)	ellipse	3.0	Aluminum
Arc	28	round	7.8	Stainless steel
Straight	47	round	4.2	Stainless steel

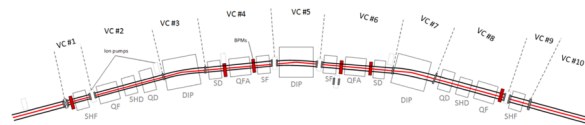


Figure 1: Layout of a normal arc section.

* Work supported by the Director Office of Science of the U. S. Department of Energy under Contract No. DE-AC02-05CH11231.

[†] dwang2@lbl.gov

Geometric Impedance

The majority of the relevant AR components have been simulated by the numerical solver CST Particle Studio. These include two RF cavities, button-type BPMs, inline pumps, pump screens, transitions between the vacuum chambers with different ID such as the transition from arc chamber to dipole chamber (“transition_AD”), or the transition from the straight section to the arc section (“transition_SA”), flanges, bellows, etc. The types and quantities of each component are listed in Table 3.

In CST simulations, EM models are built directly from the imported mechanical CAD models. CST calculates the wakefield in time domain and derives the impedance in frequency domain by Fourier transform. The CST simulation has been cross-checked with analytical formulas as much as applicable [8]. Table 2 summarizes the comparison between the value of longitudinal $\text{Im}(Z_{||}/n)$ of the inductive components in the low-frequency limit as determined with CST and analytical formulas.

Table 2: Low Frequency Limit of $\text{Im}(Z_{||}/n)$ with CST and Analytical Models [7]

Element	CST (mΩ)	Model (mΩ)
Inline pump	0.03	N/A
Pump screen	0.08	0.08
Arc pump screen	0.07	0.07
BPM	0.05	0.04
Flange	0.11	0.13
Straight Transition	2.01	2.02
Arc transition	0.85	0.76
Cavity transition	2.31	2.78
LFB transition	2.47	2.37

IMPEDANCE BUDGET

Longitudinal Budget

After calculating the short range wakefield and corresponding broad-band impedance of each components, we add them up with the quantity factor in the ring to get the total budget as shown in Fig. 2.

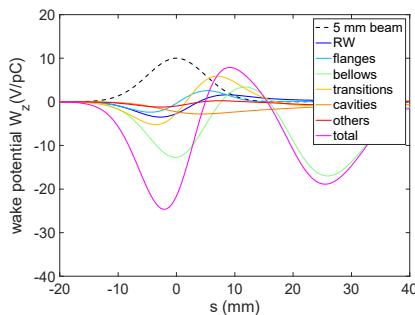


Figure 2: Short range longitudinal wakefield potential induced by the AR 5mm beam. Individual components and total (magenta)

The loss factor and normalized impedance (both real part and imaginary part) of each type of component are list in Table 3. The total loss factor is calculated as $\kappa =$

$\int_{-\infty}^{\infty} W(s)\lambda(s)ds$, and equals 13.3 V/pC for the AR 5 mm beam. The three main dominant contributions are from the bellows, RF cavities and the resistive wall. We can also get an effective impedance of each components shown in Table 3 by fitting the total short range wakefield curve against the R + L model following K.Bane’s method [9]. According to this model, the longitudinal charge distribution of the drive beam is $\lambda(s)$, then the wakefield potential curve is fitted to the sum of a purely resistive wake—yielding a wakepotential shape is similar to $\lambda(s)$, plus a purely inductive wake—yielding a wake shape is similar to the derivation of the current $\lambda'(s)$: $W_{R+L}(s) = -cR\lambda(s) - c^2L\lambda'(s)$, where R is the resistance, and L is the inductance. For the total short range wakefield we find that the fitted $R = 783.0 \Omega$, $L = 12.4$ nH. Then we can extract an effective impedance of $|Z/n|$ from the model fitting using:

$$\frac{Z}{n} = \frac{\omega_0 \sigma_z}{c} R + i\omega_0 L \quad (3)$$

having chosen ω to be a representative frequency, e.g. corresponding to the nominal bunch length $\sigma_z = 5$ mm and where $n = \omega/\omega_0$ with ω_0 the revolution frequency. We find $|Z/n| = 0.19$ in total.

Transverse Budget

Similarly, we can establish the transverse impedance budget. One of the key parameters for transverse budget is the effective impedance defined as: $z_{\perp}^{eff} = 2\sqrt{\pi}\sigma_{\tau}\kappa_{\perp}$, where σ_{τ} is the bunch length in time, and $\kappa_{\perp} = \int_{-\infty}^{\infty} \text{Im}Z_{\perp}(\omega)F(\omega)d\omega$ the transverse kick factor. The driving terms of these transverse instabilities scale as the product of the local dipole impedance with the beta function. The corresponding induced tune shift reads $\delta\nu = -Q\beta\kappa_{\perp}/(4\pi E/e)$ with $Q=1.15$ nC, and $E=2$ GeV for the AR beam. We summarize the transverse impedance budget as well as the tune shift of 5mm beam for each type of component in the AR beam in Table 3.

We show the beta-weighted imaginary part of the impedance in the vertical plane in Fig. 3. The main contribution to the tune shift comes from the transitions between dipole chamber and the arc chamber (36 transition pairs in total, from radius 7 mm to 14 mm in the vertical plane).

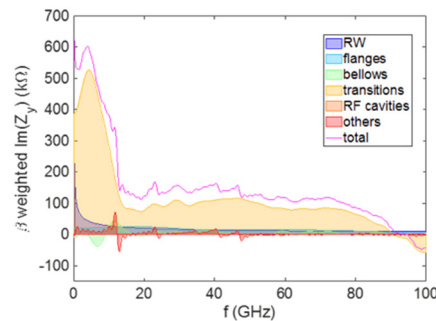


Figure 3: Beta-weighted imaginary part of the vertical impedance, for the individual components and their sum.

INSTABILITY STUDY

We apply the macro-particle simulation code *legant* to simulate beam dynamics in the presence of wakefields.

Longitudinal: Microwave Instability

legant simulations of single-bunch longitudinal dynamics indicate an 11 nC/bunch threshold for the onset of a microwave-like instability as shown in Figure 4 [10]. Simulations with a Vlasov solver (not shown here) give a very similar determination [11].

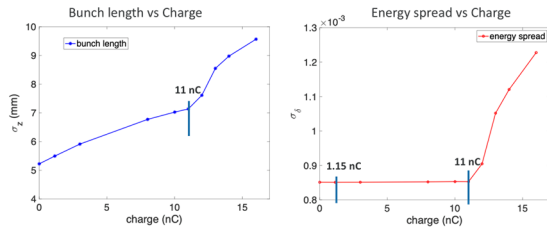


Figure 4: The rms bunch length a) and relative energy spread b) as functions of bunch charge after about 2.5 damping times (starting from the zero-current equilibrium).

Transverse Mode Coupling Instability (TMCI)

The transverse simulations are carried out with starting with a beam with an initial 1 mm offset. The evolution for the beam centroid is monitored looking for the onset of exponential growth. The instability thresholds occurs at about 12 nC/bunch as shown in Fig. 5.

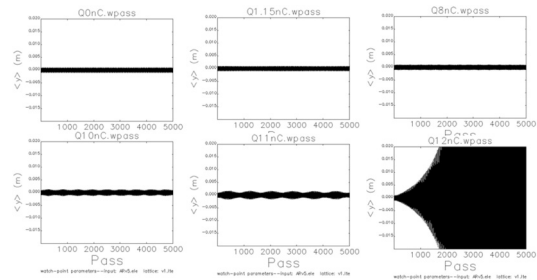


Figure 5: Bunch vertical centroid vs. no. of passes, for different bunch charge in the presence of short-range wakefields.

CONCLUSION

The broad-band impedance of the ALS-U AR has been extensively analyzed using numerical and analytical methods. The majority of the impedance sources have been considered. The impedance model will continue to be updated as the vacuum components design reaches full maturity. Based on the current impedance model, simulations show a ~10-fold margin for single bunch instability thresholds in both longitudinal and transverse planes.

ACKNOWLEDGEMENTS

We would like to thank Dr. R. Warnock from SLAC for simulations with Vlasov solver and R. Li from Jlab for helpful discussions.

Table 3: Impedance Modelling of the AR Ring for Nominal 5mm Bunch Length

Component	No.	Loss factor (V/pC)	Re(Z/n) (mΩ)	Im(Z/n) (mΩ)	(β*Z _{eff}) _x (kΩ)	(β*Z _{eff}) _y (kΩ)	Tune shift x × 10 ⁻⁴	Tune shift y × 10 ⁻⁴
Transitions_AD	36	0.14	0.66	31.37	8.74	348.70	-0.07	-2.70
Resistive wall	1	1.60	16.23	24.01	20.82	57.94	-0.16	-0.45
Transitions_SA	12	0.49	4.96	25.31	58.53	22.83	-0.45	-0.18
Flange*	240	0.08	3.13	28.41	20.66	22.40	-0.16	-0.17
Pump screen	48	0.03	0.28	5.44	1.33	17.17	-0.01	-0.13
BPM	72	0.10	1.02	2.87	6.88	10.80	-0.05	-0.08
Inline pump	48	0.01	0.06	1.55	13.31	5.62	-0.10	-0.04
Bellow*	84	8.15	82.62	21.00	10.37	4.49	-0.08	-0.04
Cavity	2	1.96	19.86	-14.19	13.83	4.61	-0.11	-0.04
Cavity transition	2	0.18	1.80	3.95	4.61	1.54	-0.04	-0.01
LFB kicker	1	0.49	4.97	-3.38	4.52	1.51	-0.04	-0.01
LFB transition	1	0.08	0.77	1.62	2.04	0.68	-0.02	-0.01
Stripline kicker	1	0.01	0.09	~ 0.00	0.51	0.17	0.00	0.00
Ring total		13.3	136.4	128.0	166.2	498.0	-1.29	-3.85

REFERENCES

- [1] C. Steier *et al.*, “Design Progress of ALS-U, the Soft X-ray Diffraction Limited Upgrade of the Advanced Light Source,” in *Proc. 10th Int. Particle Accelerator Conf. (IPAC'19)*, Melbourne, Australia, May 2019, pp. 1639-1642. doi:10.18429/JACoW-IPAC2019-TUPGW097
- [2] K. Bane *et al.*, “Impedance Calculation and Verification in Storage Rings,” SLAC-PUB-11007, 2005.
- [3] A. Blednykh and S. Krinsky, “Preliminary Impedance Budget for the NSLS-II Storage Ring”, in *Proc. 22nd Particle Accelerator Conf. (PAC'07)*, Albuquerque, NM, USA, Jun. 2007, paper FRPMS102, pp. 4321-4323.
- [4] *elegant*, https://ops.aps.anl.gov/manuals/elegant_latest/elegant.html
- [5] A. Piwinski, “Wakefields and ohmic losses in round vacuum chambers,” DESY-HERA-92-11, May 1992.
- [6] CST, <https://www.cst.com/products/cst>
- [7] K. Yokoya, “Resistive Wall Wake Function for Arbitrary Pipe Cross Section”, in *Proc. 15th Particle Accelerator Conf. (PAC'93)*, Washington D.C., USA, Mar. 1993, pp. 3441-3444.
- [8] A. Chao, *Handbook of Accelerator Physics and Engineering*, 2nd edition, World Scientific, pp. 253-263, May 2013.
- [9] K. Bane, “Longitudinal Stability Study for the FACET-II e⁺ Damping Ring,” SLAC-PUB-16879, November 2016.
- [10] K. Y. Ng, “Physics of Intensity Dependent Beam Instabilities,” Fermilab-FN-0713, 2002. <https://lss.fnal.gov/archive/test-fn/0000/fermilab-fn-0713.shtml>
- [11] R. Warnock and K. Bane, “Numerical solution of the Haïssinski equation for the equilibrium state of a stored electron beam,” *Phys. Rev. AB*, vol. 21, p. 124401, 2018.